

**THE SLOPE ASSESSMENT USING  
GEOPHYSICAL APPROACHES WITH  
INTEGRATED ANALYSIS OF 2-D CROSS PLOT  
MODEL**

**MUHAMMAD TAQUIDDIN BIN ZAKARIA**

**UNIVERSITI SAINS MALAYSIA**

**2021**

**THE SLOPE ASSESSMENT USING  
GEOPHYSICAL APPROACHES WITH  
INTEGRATED ANALYSIS OF 2-D CROSS PLOT  
MODEL**

by/oleh

**MUHAMMAD TAQIUDDIN BIN ZAKARIA**

**Thesis submitted in fulfilment of the requirements  
for the degree of  
Doctor of Philosophy**

**April 2021**

## ACKNOWLEDGEMENT

In the name of Allah S.W.T, the Most Beneficent and Merciful. First and foremost, I would like to express my thanks to God for the love and strength Allah has given me to complete this PhD's thesis successfully. I am thankful for Allah's blessings throughout my daily life and good health. I want to take this opportunity to convey my gratitude to my supervisor, Dr. Nordiana binti Mohd Muztaza, who had spent her valuable time guiding and giving me chance to improve my knowledge despite her busy schedule. She had been very patience and enthusiastic when giving me encouragement and critiques, which proved extremely useful when doing this research until the end. My sincere thanks also go to my co-supervisor, Associate Professor Dr. Hareyani binti Zabidi, for the aspiring guidance and insightful comments throughout my study. Thanks to all of the Geophysics laboratory staff, especially Mr. Shahil bin Ahmad Khosaini, Mr. Zulkeflee bin Ismail, Mr. Azmi bin Abdullah, and a technician of the School of Material and Mineral Resources, Mr. Saarani bin Ijak who gave full commitment and access to the laboratory and research facilities. Without their precious support, it would not be possible to conduct this research. Not to forget, my deepest thanks and appreciation to my fellow postgraduate students who had been very helpful in sharing their knowledge and experiences; Mr. Adeeko Tajudeen Olugbenga, Ms. Alyaa Nadhirah binti Salleh, Ms. Nazirah binti Mahmud, Ms. Nurina Auni binti Ismail, Ms. Nuraisyah binti Samsudin, Mr. Farid Najmi bin Rosli, Mr. Mustapha Adejo Mohammed, Mr. Mark bin Jinmin, Mr. Kiu Yap Chong, Mr. Rais bin Jusoh, Mr. Nazrin bin Rahman, and Mrs. Najmiah binti Rosli. Special thanks also to undergraduate student Ms. Alisha binti Akram, and Ms. Fitriah binti Zaidi. I would like to recognize the invaluable assistance that you all provided during my study. May

Allah shower the above-cited personalities with success and honour in their life. I wish to acknowledge the support and great love of my beloved parents Zakaria bin Ishak and Siti Selamah binti Junus, my sister Norsafinah binti Zakaria and my brother Taufif bin Zakaria for providing me with unfailing support and continuous encouragement throughout my years of study and through the process of researching and writing this thesis. This accomplishment would not have been possible without them. Thank you. I also want to thank Universiti Sains Malaysia (USM) for offering the scholarship scheme of the USM Fellowship and Majlis Amanah Rakyat (MARA) for providing the Graduate Excellence Programme (GrEP). Thank you to USM for providing the Fundamental Research Grant Scheme (FRGS) of Development of 2-D Linear Inversion Algorithm from Geophysical Approach for Soil or Rock Characteristics (203/PFIZIK/6711663), and the Research University Grant (RUI) entitled Geophysical Application and Approaches in Engineering and Environmental Problems (1001/PFIZIK/811323) and Integrated Geophysical Characterization of Geothermal Exploration and Strategy for A Sustainable Use of Geothermal Resources (100/PFIZIK/8011110) for supported research data acquisition. Lastly, I want to thank those not mentioned here for give me the strength to complete this PhD's journey. I wish to thank all the people whose assistance was a milestone in the completion of this thesis.

## TABLE OF CONTENTS

<b>ACKNOWLEDGEMENT</b> .....	<b>ii</b>
<b>TABLE OF CONTENTS</b> .....	<b>iv</b>
<b>LIST OF TABLES</b> .....	<b>viii</b>
<b>LIST OF FIGURES</b> .....	<b>x</b>
<b>LIST OF SYMBOLS</b> .....	<b>xviii</b>
<b>LIST OF ABBREVIATIONS</b> .....	<b>xxi</b>
<b>LIST OF APPENDICES</b> .....	<b>xxii</b>
<b>ABSTRAK</b> .....	<b>xxiii</b>
<b>ABSTRACT</b> .....	<b>xxv</b>
<b>CHAPTER 1 INTRODUCTION</b> .....	<b>1</b>
1.1 Introduction .....	1
1.2 Landslide overview .....	2
1.3 Problem statement .....	4
1.4 Objective of the research .....	5
1.5 Scope of the research.....	6
1.6 Novelty of the research.....	7
1.7 Thesis outline .....	7
<b>CHAPTER 2 LITERATURE REVIEW</b> .....	<b>9</b>
2.1 Introduction .....	9
2.2 Basic theory of resistivity .....	10
2.3 Basic theory of seismic refraction .....	13
2.4 Basic theory of multi-channel analysis of surface wave (MASW) .....	14
2.5 Elastic moduli for subsurface characterisation.....	16
2.6 Shear strength of the soil .....	18
2.7 Overview of landslide in Malaysia.....	19

2.8	Previous study .....	21
2.8.1	Overview of landslide assessment .....	21
2.8.2	Cross-plot analysis .....	29
2.9	Chapter summary .....	31
<b>CHAPTER 3 METHODOLOGY .....</b>		<b>33</b>
3.1	Introduction .....	33
3.2	Background and geology of study areas.....	34
3.2.1	USM-Archaeology (Stable slope, St).....	35
3.2.1(a)	Field procedure.....	37
3.2.2	Lojing-Cameron Highland (Critical slope, Cr) .....	37
3.2.2(a)	Field procedure.....	41
3.2.3	Hulu Yam (Failure slope, Fa) .....	41
3.2.3(a)	Field procedure.....	44
3.2.4	Bkt Antarabangsa (Failure slope, Fa) .....	44
3.2.4(a)	Field procedure.....	48
3.3	Geophysical methods .....	48
3.3.1	2-D resistivity.....	49
3.3.1(a)	2-D Resistivity data processing.....	54
3.3.2	Seismic refraction .....	56
3.3.2(a)	Seismic refraction data processing.....	59
3.3.3	MASW .....	60
3.3.3(a)	MASW data processing.....	64
3.3.3(b)	Combined dispersion curve.....	67
3.4	Geotechnical investigation .....	70
3.4.1	Hand-auger.....	70
3.4.2	Soil bulk density test.....	71
3.4.3	Direct shear box test.....	71

3.5	Cross-plot analysis of geophysical data .....	75
3.6	Volume estimation of mass sliding .....	82
3.7	Chapter summary .....	83
<b>CHAPTER 4 RESULTS AND DISCUSSION .....</b>		<b>85</b>
4.1	Introduction .....	85
4.2	Phase I .....	85
4.2.1	Stable slope (USM-Archaeology) .....	85
4.2.1(a)	2-D resistivity .....	85
4.2.1(b)	Seismic refraction and MASW .....	88
4.2.1(c)	Integration of geophysical methods .....	98
4.2.1(d)	Modulus estimation using integrated $V_p$ - $V_s$ .....	102
4.2.2	Critical slope (Lojing-Cameron Highland) .....	105
4.2.2(a)	2-D resistivity .....	105
4.2.2(b)	Seismic refraction and MASW .....	109
4.2.2(c)	Integration of geophysical methods .....	114
4.2.2(d)	Modulus estimation using integrated $V_p$ - $V_s$ .....	120
4.2.3	Failure slope (Hulu Yam and Bkt Antarabangsa) .....	122
4.2.3(a)	Hulu Yam .....	122
4.2.3(a)(i)	2-D resistivity of Hulu Yam .....	123
4.2.3(a)(ii)	Seismic refraction of Hulu Yam .....	125
4.2.3(a)(iii)	Integration of geophysical methods .....	127
4.2.3(b)	Bkt Antarabangsa .....	138
4.2.3(b)(i)	2-D resistivity of Bkt Antarabangsa .....	138
4.2.3(b)(ii)	Seismic refraction of Bkt Antarabangsa .....	144
4.2.3(b)(iii)	Integration of geophysical methods .....	145
4.2.4	Direct shear box test .....	157
4.2.4(a)	Stable slope (USM-Archaeology) .....	158
4.2.4(b)	Critical slope (Lojing) .....	160

4.3	Phase II.....	161
4.3.1	Integration of resistivity and seismic using cross-plot analysis...	162
4.3.1(a)	USM-Rumah Tamu (Test model) .....	162
4.3.1(b)	Lojing-Cameron Highland (Critical slope) .....	169
4.3.1(c)	Hulu Yam (Failure slope).....	174
4.3.1(d)	Bkt Antarabangsa (Failure slope).....	179
4.3.2	Volume estimation of mass sliding.....	184
4.3.2(a)	Critical slope (Lojing-Cameron Highland) .....	184
4.3.2(b)	Failure slope (Hulu Yam & Bkt Antarabangsa).....	186
4.4	Chapter summary .....	189
4.4.1	Phase I.....	190
4.4.2	Phase II.....	193
<b>CHAPTER 5 CONCLUSION AND FUTURE RECOMMENDATIONS .</b>		<b>196</b>
5.1	Conclusion.....	196
5.2	Recommendations for future research.....	199
<b>REFERENCES .....</b>		<b>200</b>
<b>APPENDICES</b>		
<b>LIST OF PUBLICATIONS</b>		



## LIST OF TABLES

		<b>Page</b>
Table 2.1	General values of shear modulus for several soil types (Sabatini et al., 2002).....	17
Table 2.2	General values of the Poisson's Ratio for several soil types (Braja, 2008) .....	18
Table 2.3	Shearing angle of friction for soil types (Whitlow, 2004) .....	19
Table 2.4	Reported cases of landslide in Malaysia in year of 2000-2006 (Gue & Tan, 2007) .....	21
Table 3.1	Survey lines of USM.....	37
Table 3.2	Survey lines of Lojing.....	41
Table 3.3	Survey lines of Hulu Yam.....	44
Table 3.4	Survey lines of Bkt Antarabangsa.....	48
Table 3.5	The median depth of investigation ( $Z_e$ ) for different array (Edwards, 1977; Loke, 2015).....	53
Table 3.6	SAS4000 2-D resistivity acquisition parameters .....	54
Table 3.7	Shot point of survey lines for each study area .....	58
Table 3.8	General parameter settings of Terraloc MK8 seismograph .....	58
Table 3.9	Shot point location of the survey lines at USM and Lojing areas.....	62
Table 3.10	General setting of Terraloc MK8 seismograph for MASW.....	63
Table 3.11	The example of quadrant limit of resistivity and velocity .....	79
Table 4.1	Summary of coefficient of determination of $R^2$ between $V_s$ and $V_p$ .....	94
Table 4.2	Summary of coefficient of determination of $R^2$ between $V_s$ and $V_p$ .....	111
Table 4.3	Result of direct shear box test at USM.....	159

Table 4.4	Result of direct shear box test at Lojing.....	161
Table 4.5	Geophysical survey of USM-Rumah Tamu.....	163
Table 4.6	The summary of volume calculation of mass sliding for critical slope .....	186
Table 4.7	The summary of volume calculation of mass sliding for failure slope .....	189
Table 4.8	The summary of Phase I.....	193
Table 4.9	The summary of Phase II .....	195

## LIST OF FIGURES

	<b>Page</b>
Figure 1.1	An overview of rainfall-landslide mechanism (Yeong, 2012).....4
Figure 2.1	Schematic diagram of a landslide system, showing the major landslide setting features that can be investigated and assessed using geophysical methods (Whitley et al., 2019) ..... 10
Figure 2.2	Electrical resistivity with the relation of resistance (R), area (A), and length (L)..... 11
Figure 2.3	A conventional four-electrode array (Loke, 2015) ..... 11
Figure 2.4	Common array used in an electrical survey with different geometric factor (Loke, 2015)..... 12
Figure 2.5	Illustration of current flow in the homogeneous subsurface (modified from Loke, 2015)..... 12
Figure 2.6	Travel time of seismic waves ..... 14
Figure 2.7	Rayleigh wave component with different wavelength propagating through a layered medium. Wave components with different frequency reflect soil properties at diverse depth ..... 15
Figure 2.8	Mohr-Coulomb failure criterion..... 19
Figure 3.1	Framework of research workflow ..... 34
Figure 3.2	3-D topography of USM-Archaeology (source: Google Earth)..... 35
Figure 3.3	Geomorphology of study area of USM: a) Survey lines; b) Google Earth image; c) Geological map..... 36
Figure 3.4	3-D topography of Lojing-Cameron Highland (source: Google Earth)..... 39
Figure 3.5	Geomorphology map of study area of Lojing: a) Survey lines; b) Geological map; c) Google Earth image; d) 2-D cross section..... 40
Figure 3.6	3-D topography of Hulu Yam (source: Google Earth)..... 42

Figure 3.7	Geomorphology map of study area of Hulu Yam: a) Survey lines; b) Geological map; c) Google Earth image.....	43
Figure 3.8	3-D topography of Bkt Antarabangsa (source: Google Earth).....	46
Figure 3.9	Geomorphology map of study area of Bkt Antarabangsa: a) Survey lines; b) Geological map; c) Google Earth image.....	47
Figure 3.10	Electrode arrangement for resistivity array: a) Wenner-Schlumberger; b) Pole-dipole .....	51
Figure 3.11	Configuration of resistivity measurement using Wenner-Schlumberger array .....	51
Figure 3.12	Roll-along technique for two cables .....	51
Figure 3.13	Flow chart of 2-D resistivity data processing .....	55
Figure 3.14	Generated results of Res2Dinv for URI in USM study area; a) Apparent resistivity from the field, b) Calculated apparent resistivity from software, c) True resistivity value from inversion process.....	56
Figure 3.15	Schematic diagram of seismic refraction method .....	57
Figure 3.17	Flow chart of seismic refraction data processing.....	60
Figure 3.18	Roll-along technique for MASW data measurement.....	61
Figure 3.19	Signal transformation from (x-t) domain to (f-k) domain using f-k transform: a) Signal responses in the time domain; b) Overtone or dispersion image.....	65
Figure 3.20	The DINVER program for inversion analysis. The red dashes box shows the dispersion curve information in slowness-frequency displays while yellow dashes box shows the inversion information with minimum misfit.....	67
Figure 3.21	Flow chart of general MASW data processing .....	67
Figure 3.22	The dispersion curve and final velocity profiles; a) Average dispersion curve from two identical dispersion curves of the same mid-point location with different shot point locations (-ve offset). The blue, green, and red curves represent Curve 1, Curve 2, and	

	average curve, respectively; b) The final velocity profiles for Lojing area of line LM3 at different mid-point locations (S1-S4).....	69
Figure 3.23	The steps involved in dispersion curves combination.....	69
Figure 3.24	Component of AMS hand-auger tool.....	70
Figure 3.25	Shear-strain relationship; a) Stress-displacement plot; b) Shear stress ( $\tau_p$ )-normal stress plot ( $\sigma'_f$ ).....	74
Figure 3.26	Direct shear box test; a) The shear box test equipment from VJAY; b) The preparation of the remoulded specimen; c) The final specimen after compaction.....	74
Figure 3.27	Schematic relationship from Hayashi and Konishi model (2010) models of cross-plot analysis .....	76
Figure 3.28	Schematic relationship of resistivity-P-wave velocity.....	76
Figure 3.29	The comparison of total datum point: a) *.grd* file; b) raw file.....	78
Figure 3.30	The graphical analysis with sorted of x-y position; a) The unfiltered data from both resistivity and velocity data; b) The filtered data based on the range distribution of the results, (insignificant data with extremely high values were removed) .....	78
Figure 3.31	Resistivity-velocity plot with quadrants display. The lower limit and upper limit were used to classify the values accordingly .....	80
Figure 3.32	2-D cross-plot model based on the resistivity-velocity values range .....	80
Figure 3.33	Workflow of cross-plot analysis .....	81
Figure 3.34	Graphical illustration of volumetric mass movement determination .....	83
Figure 4.1	Inversion models of 2-D resistivity of USM area; a) UR1; b) UR2; c) UR3; d) UR4; e) UR5; f) UR6.....	87
Figure 4.2	Seismic refraction models and 1-D MASW profiles of the USM area for US1 & UM1 .....	90

Figure 4.3	Seismic refraction models and 1-D MASW profiles of the USM area for US2 & UM2-US3 & UM3.....	91
Figure 4.4	Seismic refraction models and 1-D MASW profiles of the USM area for US4 & UM4-US5 & UM5.....	92
Figure 4.5	Correlations between $V_p$ and $V_s$ for line US1 & UM1 and line US2 & UM2 .....	95
Figure 4.6	Correlations between $V_p$ and $V_s$ for line US3 & UM3 and line US4 & UM4 .....	96
Figure 4.7	Correlations between $V_p$ and $V_s$ for line US5 & UM5.....	97
Figure 4.8	Integration of 2-D resistivity and seismic refraction models; a) UR1&US1; b) UR2&US2; c) UR3&US3; d) UR4& US4; e) UR5& US5; f) 3-D orientation of 2-D resistivity for all profiles; g) 3-D orientation of seismic refraction for all profiles .....	100
Figure 4.9	1-D MASW profiles for lines UM1-UM5 .....	102
Figure 4.10	Shear and Young's moduli distribution for USM area .....	103
Figure 4.11	Correlation between shear modulus and Young's modulus.....	104
Figure 4.12	Poisson's ratio distribution of USM.....	105
Figure 4.13	Velocity ratio ( $V_p/V_s$ ) vs Poisson's ratio distribution of USM .....	105
Figure 4.14	Inversion models of 2-D resistivity of Lojing area; a) LR4; b) LR3; c) LR2; d) LR4.....	108
Figure 4.15	Inversion models of 2-D resistivity of Lojing area of lines LR4-LR1.....	108
Figure 4.16	Seismic refraction models of Lojing area; a) LS4; b) LS3; c) LS2; d) LS4.....	110
Figure 4.17	Seismic refraction models and 1-D MASW profiles of the study area; a) LS4; b) LS2; c) LM4; d) LM2 .....	112
Figure 4.18	Correlation between $V_p$ and $V_s$ for line LS4&LM4 and LS2&LM2 .....	113

Figure 4.19	Integration of 2-D resistivity and seismic refraction models; a) LR4&LS4; b) LR3&LS3; c) LR2&LS2; d) LR1&LS1; e) 3-D orientation of 2-D resistivity for all profiles; f) 3-D orientation of seismic refraction for all profiles .....	118
Figure 4.20	1-D MASW profiles for lines LM4 & LM2.....	119
Figure 4.21	Shear and Young's modulus distribution for Lojing area.....	120
Figure 4.22	Correlation relation between Shear modulus and Young's modulus .....	121
Figure 4.23	Poisson's ratio distribution in Lojing.....	122
Figure 4.24	Velocity ratio ( $V_p/V_s$ ) vs Poisson's ratio distribution in Lojing .....	122
Figure 4.25	Inversion models of 2-D resistivity of Hulu Yam area: a) HR1; b) HR2; c) HR4; d) HR3; e) HR5; f) HR6 .....	125
Figure 4.26	Seismic refraction models of Hulu Yam area; a) HS1; b) HS2; c) HS3.....	126
Figure 4.27	Integration of 2-D resistivity and seismic refraction models; a) HR1&HS1; b) HR2&HS2; c) HR4&HS3.....	129
Figure 4.28	Integrated result of geophysical models and borehole record; a) Line HR1&HS1 with BH10; b) Line HR1&HS2 with BH9.....	132
Figure 4.29	3-D model of resistivity result with Gapis river pathway .....	135
Figure 4.30	Rainfall distribution for Hulu Yam landslide; a) Overview rainfall distribution throughout the year; b) Daily rainfall distribution within 3 months (Sept-Nov); c) 30 days' cumulative rainfall amount for November month.....	137
Figure 4.31	Inversion models of 2-D resistivity of Bkt Antarabangsa- parallel to the slope ( <i>outside from landslide boundary</i> ); a) BR1; b) BR2; c) BR9; d) BR4; e) BR6.....	140
Figure 4.32	Inversion models of 2-D resistivity of Bkt Antarabangsa-parallel to the slope ( <i>inside landslide area</i> ); a) BR3; b) BR5; c) BR7; d) BR8 .....	142

Figure 4.33	Inversion models of 2-D resistivity of Bkt Antarabangsa ( <i>perpendicular lines to the slope</i> ); a) BR12; b) BR10; c) BR14; d) BR11; e) BR13.....	144
Figure 4.34	Seismic refraction models of Bkt Antarabangsa; a) BS1; b) BS2; c) BS3.....	145
Figure 4.35	Integration of 2-D resistivity and seismic refraction models; a) BR11&BS3; b) BR2&BS1; c) BR7&BS2.....	148
Figure 4.36	Integrated result of geophysical models and borehole record; a) BR2&BS1-BH8; b) BR3-BH6, c) BR4-BH4; d) BR5-BH25; e) BR9-BH1; f) BR12-BH23; g) BR13-BH12-BH16.....	153
Figure 4.37	3-D orientation of 2-D resistivity for S-N and W-E direction.....	154
Figure 4.38	Rainfall distribution for Bkt Antarabangsa landslide; a) Overview rainfall distribution throughout the year; b) Daily rainfall distribution within 3 months (Nov-Dec); c) 30 days' cumulative rainfall amount from 6 Nov-6 Dec 2008.....	157
Figure 4.39	Shear stress-normal stress graph of USM-Archaeology at depth; a) 1.0 m; b) 2.0 m; c) 3.0m.....	160
Figure 4.40	Shear stress-normal stress graph of Lojing at depth; a) 0.5 m; b) 1.0 m.....	161
Figure 4.41	Schematic diagram of the layout USM-Rumah Tamu.....	163
Figure 4.42	The result of USM-Rumah Tamu; a) The geophysical result of 2-D resistivity and seismic refraction; b) The correlated geophysical result with borehole record for BH2; c) The correlated geophysical result with borehole record for BH1 .....	165
Figure 4.43	The graph analysis of geophysical parameters with borehole data of BH2; a) Velocity-N value versus depth; b) Resistivity-N value versus depth.....	167
Figure 4.44	The graph analysis of geophysical parameters with borehole data of BH1; a) Velocity-N value versus depth; b) Resistivity-N value versus depth.....	167



Figure 4.45	The cross-plot analysis based on the integration between 2-D resistivity and seismic refraction models; a) The initial models of 2-D resistivity and seismic refraction; b) The datum point distribution of 2-D resistivity and seismic refraction models; c) The overlapped datum point of both 2-D resistivity and seismic refraction; d) The cross-plot datum point of both methods after geometry correction; e) The graphical analysis based on threshold values; f) The example of final output of 2-D cross-plot model.....	169
Figure 4.46	Graph integration of resistivity-velocity for the same X–Y location a) LR4&LS4; b) LR3&LS3; c) LR2&LS2; d) LR1&LS1 .....	171
Figure 4.47	The 2-D cross-plot model; a) LR4&LS4; b) LR3&LS3; c) LR2&LS2; d) LR1&LS1; e) 2-D Schematic profile of Lojing with depth to failure plane.....	174
Figure 4.48	Graph integration of resistivity-velocity for the same X–Y location; a) HR1&HS1; b) HR2&HS2; c) HR4&HS3.....	175
Figure 4.49	2-D cross-plot model of integrated 2-D resistivity and seismic refraction: a) HR1& HS1; b) HR2&HS2; c) HR4&HS3 .....	178
Figure 4.50	Graph integration of resistivity-velocity for the same X–Y location; a) BR11&BS3; b) BR2&BS1; c) BR7&BS2.....	180
Figure 4.51	2-D cross-plot model of integrated 2-D resistivity and seismic refraction: a) BR11& BS3; b) BR2&BS1; c) BR7&BS2 .....	183
Figure 4.52	Elevation map of Lojing study areas; a) Surface elevation map of study area; b) Extracted upper surface elevation of creep area; c) Extracted lower surface of sliding plane at creep area.....	185
Figure 4.53	Volume calculation of mass sliding at Lojing study area; a) 3-D illustration of volume of mass sliding calculation between two different maps (Upper-Lower); b) 3-D isopach map of mass sliding after the calculation .....	185
Figure 4.54	Elevation map of Hulu Yam study areas; a) Surface elevation map of study area; b) Extracted upper surface elevation of landslide area; c) Extracted lower surface of sliding plane at landslide area ..	187

Figure 4.55	Volume calculation of mass sliding at landslide Hulu Yam study area; a) 3-D illustration of volume of mass sliding calculation between two different maps (Upper-Lower); b) 3-D isopach map of mass sliding after the calculation.....	187
Figure 4.56	Elevation map of Bkt Antarabangsa study areas; a) Surface elevation map of study area; b) Extracted upper surface elevation of landslide area; c) Extracted lower surface of sliding plane at landslide area.....	188
Figure 4.57	Volume calculation of mass sliding at landslide Bkt Antarabangsa study area; a) 3-D illustration of volume of mass sliding calculation between two different maps (Upper-Lower); b) 3-D isopach map of mass sliding after the calculation.....	189

## LIST OF SYMBOLS

A	Cross-sectional area
a	Electrode spacing
c	Cohesion
c'	Cohesion in term of effective stress
C1	Current electrode 1
$c_p$	Phase velocity
Cr	Critical slope
dx	Receiver spacing of geophones
E	Young's modulus
f	Frequency
Fa	Failure slope
f-k	Frequency-wave number
$g/cm^3$	Gram per centimeter cube
$G_0$	Shear modulus
GPa	Gigapascal
ha	hectares
Hz	Hertz
I	Current
$i_c$	Critical angle
k	Geometric factor
$k$	Wavenumber
kg	Kilogram
L	Length
m/s	meter per second

$m_0$	Initial mass
$mA$	Milli-ampere
$m_d$	Dry mass
$n$	Dipole separation factor
$N$	Newton
$P$	Horizontal shear force
$P1$	Potential electrode 1
$R$	Resistance
$sec$	Second
$St$	Stable slope
$t_{cross}$	Intercept time at cross-over distance
$t_i$	Intercept time
$t-x$	Time-space
$V$	Volume
$V_1$	Velocity of the first layer
$V_2$	Velocity of the second layer
$V_g$	Voltage
$V_{mm}$	Volume of mass movement
$V_p$	P-wave velocity
$V_R$	Rayleigh wave
$V_r$	Rayleigh wave phase velocity
$V_s$	S-wave velocity
$V_{sm}$	Volume of the mass body below the sliding plane
$V_{soil}$	Volume of soil
$V_{s-v}$	S-wave velocity-vertical component
$V_{tm}$	Volume of total mass body
$W_{dry}$	Weight of dry soil

$x,y$	Areal extent of landslide
$x_1$	Distance of source to receiver
$x_c$	Critical distance
$x_{cross}$	Cross-over distance
$z$	Depth
$Z_e$	Median depth of investigation
$Z_{max}$	Maximum depth of investigation
$\lambda$	Wavelength
$\lambda_{max}$	Longest wavelength
$\mu s$	Micro-seconds
$\nu$	Poisson's ratio
$\rho$	Density
$\rho$	Resistivity
$\rho_a$	Apparent resistivity
$\sigma$	Normal stress
$\sigma'_f$	Effective normal stress
$\tau$	Stress on the surface of shear
$\phi$	Angle of internal friction
$\phi'$	Angle of internal friction in term effective stress
$\Omega m$	Ohm.meter
$\tau_f$	Shear stress at failure
$\tau_p$	Peak shear stress at failure

## LIST OF ABBREVIATIONS

ABEM	Aktiebolaget Elektrisk Malmletning
BD	Bulk density
JMG	Jabatan Mineral Dan Geosains Malaysia
JMM	Jabatan Meteorologi Malaysia
MASW	Multichannel Analysis of Surface Waves
Q	Quadrant
RQD	Rock quality designation
S/N	Signal to noise ratio
SAS	Signal Averaging System
SPT	Standard Penetration Test
1-D	One dimensional
2-D	Two dimensional
3-D	Three dimensional

## **LIST OF APPENDICES**

- APPENDIX A     BOREHOLE RECORD OF USM-RUMAH TAMU
- APPENDIX B     BOREHOLE RECORD OF HULU YAM
- APPENDIX C     BOREHOLE RECORDS OF BKT ANTARABANGSA
- APPENDIX D     DAILY RAINFALL AMOUNT OF HULU YAM
- APPENDIX E     DAILY RAINFALL AMOUNT OF BKT  
ANTARABANGSA
- APPENDIX F     CROSS-PLOT MODEL OF  $C_r$  AND  $F_a$  SLOPES
- APPENDIX G     LANDSLIDE PHOTOS

**PENILAIAN CERUN MENGGUNAKAN PENDEKATAN GEOFIZIK  
BERSAMA PENGANALISAAN BERSEPADU 2-D MODEL PLOT SILANG**

**ABSTRAK**

Resolusi yang tidak mencukupi dengan kaedah-kaedah yang terhad terdedah kepada kesilapan tafsiran kerana pencirian tanah runtuh memerlukan julat data dan pemerhatian yang luas. Pengesahan dari parameter-parameter yang berbeza diperlukan untuk mengesahkan keputusan bagi mengurangkan kesalahan semasa tafsiran. Analisis plot-silang bersepadu telah diperkenalkan sebagai kaedah alternatif untuk meningkatkan tafsiran subpermukaan berdasarkan kriteria model-model. Kaedah geofizik keberintangan 2-D, pembiasan seismik, dan MASW telah digunakan untuk mencirikan perilaku tanah runtuh dengan data yang disokong dari parameter-parameter geoteknik dan hidrologi. Tiga jenis keadaan cerun dipilih, iaitu cerun stabil (*USM Arkeologi–USM*), cerun kritikal (*Lojing–LJ*), dan cerun gagal (*Hulu Yam–HY & Bkt Antarabangsa–BA*). *USM* mewakili keadaan cerun yang stabil di mana tanah jeleket dikenal pasti pada keberintangan,  $\rho=400-1000 \Omega\text{m}$  dan halaju  $V_p=800-1800 \text{ m/s}$ ;  $V_s= 250-350 \text{ m/s}$  pada kedalaman 5-10 m. Modulus anjal menunjukkan kekuatan tanah dengan moduli rendah, ( $G_0<0.1 \text{ GPa}$ ;  $E<0.25 \text{ GPa}$ ;  $\nu= 0.05-0.45$ ) dengan kedalaman  $<5 \text{ m}$ . Modulus anjal meningkat dengan kedalaman kerana parameter-parameter kekuatan ricih menunjukkan julat nilai yang tinggi ( $c'=5-29 \text{ kPa}$ ;  $\phi'= 21-28.8^\circ$ ). Dalam cerun kritikal (*LJ*), tanah sisa telah dikenal pasti sebagai bahan peroi/terluluhawa dengan keberintangan,  $\rho=200-450 \Omega\text{m}$  dan halaju,  $V_p=400-600 \text{ m/s}$ ;  $V_s= 150-200 \text{ m/s}$  pada kedalaman  $<5 \text{ m}$ . Nilai rendah moduli ( $G_0<0.1 \text{ GPa}$ ;  $E<0.25 \text{ GPa}$ ;  $\nu= 0.35-0.45$ ) dengan kedalaman  $<5 \text{ m}$ , dikaitkan dengan luluhawa tanah dengan pengurangan parameter-parameter kekuatan ricih. Cerun gagal seperti *HY* dan *BA*



menunjukkan zon luluhawa tinggi ( $\rho < 1200 \text{ } \Omega\text{m}$ ;  $V_p < 1200 \text{ m/s}$ ) dikenal pasti pada kedalaman  $< 5 \text{ m}$ . Nilai SPT-N menunjukkan julat rendah 1-15 ketukan, mewakili kekakuan rendah untuk keadaan tanah. Jumlah curahan hujan anteseden yang tinggi ( $HY = 267 \text{ mm}$ ;  $BA = 410.4 \text{ mm}$ ) menunjukkan faktor tambahan mencetuskan kejadian tanah runtuh. Model 2-D plot silang berjaya mendedahkan zon lemah dan kedalaman permukaan gelincir ( $LJ \& HY < 5 \text{ m}$ ;  $BA < 10 \text{ m}$ ) tanah runtuh. Model 2-D plot silang memberikan tafsiran komprehensif di mana kuadran, Q1 menunjukkan zon rentan badan tanah runtuh. Satah lemah berjaya dikenal pasti berdasarkan model plot silang dimana zon terluluhawa dan ciri-ciri subpermukaan ditentukan. Penganggaran isipadu pergerakan jisim berjaya dihitung untuk cerun kritikal dan gagal menggunakan peta isopak berdasarkan penentuan satah geluncur. Penganggaran isipadu masing-masing adalah  $13657.26 \text{ m}^3$ ,  $554057.83 \text{ m}^3$  dan  $167963.71 \text{ m}^3$  untuk  $LJ$ ,  $BA$  dan  $HY$ .

# THE SLOPE ASSESSMENT USING GEOPHYSICAL APPROACHES WITH INTEGRATED ANALYSIS OF 2-D CROSS PLOT MODEL

## ABSTRACT

Inadequate resolution with limitation of the methods vulnerable for misinterpretations as characterisation of landslide required a wide range of data and observations. Validation from different parameters necessary to substantiate the result as to reduce erroneous during interpretations. Integrated cross-plot analysis was introduced as an alternative method to enhance the subsurface interpretations based on the models' criteria. Geophysical methods of 2-D resistivity, seismic refraction, and MASW was utilized to characterize the landslide behaviour with supported data from geotechnical and hydrological parameters. Three types of slope conditions were selected, which are the stable slope (*USM Archaeology–USM*), the critical slope (*Lojing–LJ*), and the failure slope (*Hulu Yam–HY & Bkt Antarabangsa–BA*). *USM* represent the stable slope condition where cohesive soil were identified at resistivity,  $\rho=400-1000 \Omega\text{m}$  and velocity,  $V_p=800-1800 \text{ m/s}$ ;  $V_s= 250-350 \text{ m/s}$  at a depth of 5-10 m. Elastic modulus shows the strength of soil with low moduli ( $G_o<0.1 \text{ GPa}$ ;  $E<0.25 \text{ GPa}$ ;  $\nu = 0.05-0.45$ ) with a depth of  $<5 \text{ m}$ . The elastic modulus increases with the depth as shear strength parameters show high range values ( $c'=5-29 \text{ kPa}$ ;  $\phi'= 21-28.8^\circ$ ). In critical slope (*LJ*), the residual soil was identified as unconsolidated/weathered material with resistivity,  $\rho=200-450 \Omega\text{m}$ ) and velocity,  $V_p=400-600 \text{ m/s}$ ;  $V_s= 150-200 \text{ m/s}$  at depth of  $<5 \text{ m}$ . The low values of the moduli ( $G_o<0.1 \text{ GPa}$ ;  $E<0.25 \text{ GPa}$ ;  $\nu= 0.35-0.45$ ) at a depth of  $<5 \text{ m}$  attributed to soil weathering with reducing shear strength parameters. The failure slope of *HY* and *BA* shows a highly weathered zone ( $\rho<1200 \Omega\text{m}$ ;  $V_p<1200 \text{ m/s}$ ) was identified with a depth of  $<5 \text{ m}$ . The SPT-N values show a

low range of 1-15 blows, which represent the low stiffness of the soil condition. A high amount of antecedent rainfall ( $HY=267$  mm;  $BA=410.4$  mm) shows an additional factor triggering the landslide event. The 2-D cross plot model successfully revealed the weak zone and depth of the slip surface ( $LJ\&HY < 5$  m;  $BA < 10$  m) of the landslides. The 2-D cross-plot model gives a comprehensive interpretation where quadrant, Q1 shows the vulnerable zones of landslide body. The plane weakness was successfully identified based on the cross-plot model as the weathered zone, and subsurface features is determined. The mass movement's estimated volume was successfully calculated for critical and failure slope using the isopach map based on the sliding plane's determination. The estimated volume is  $13657.26\text{ m}^3$ ,  $554057.83\text{ m}^3$  and  $167963.71\text{ m}^3$  for  $LJ$ ,  $BA$  and  $HY$ , respectively.

# CHAPTER 1

## INTRODUCTION

### 1.1 Introduction

Landslides or unstable slopes are complex geological events with high socio-economic impacts in populated regions of many countries causing severe damages in term of lives lost and facilities destroyed. Landslides are known as 'mass-wasting' which occurs due to the down-slope movement of soil and rock in a large variety of shapes and volume (Rahman & Mapjabil, 2017; Morelli et al., 2019). Although the impact of this geo-hazard is inevitable, it can be significantly reduced by increasing the capacity to assess and predict the risks using different mitigation methods (Morelli et al., 2019). In the past decades, numerous modelling methods have been designed to assess slope stability, predict slope response to various triggers and evaluate slope deformation (Morelli et al., 2019). Investigation of subsurface landslide features is necessary to provide preliminary input for forward modelling and subsequent predictions of potential failure events (Malet et al., 2005; Rosso et al., 2006). However, such models still require access to detailed information of geological, mechanical, hydrogeological properties and boundaries conditions. Identification of the factors which control the landslide mechanism with a high spatial resolution becomes one of the challenges in landslides characterisations (Travelletti & Malet, 2012). The behaviour of slope involves the mechanical properties of soil which is an essential aspect that needs to be considered. Slope failures analysis and stabilisation require an understanding and evaluation of the processes that govern the behaviour of the slopes (Ozcep et al., 2010). Comprehensive result with proper numerical modelling helps to develop the predictive model, especially for complex landslides event.

Hence, several geophysical approaches with soil mechanics laboratory analysis were applied to study soil characteristic of failure zones. 2-D resistivity, seismic refraction and multichannel analysis of surface wave (MASW) were used to delineate the soil properties. Geotechnical and hydrological parameters were used as supporting information in providing realistic data interpretation. In this research, three major conditions of slope behaviour were classified based on the slope condition; stable, critical and failure slope. The classification was based on the geomorphology observations where slope with no active slope modification occurred was considered as stable slope for. The critical condition was defined as where there is active slope/soil movement exhibit the instability whereas the failure slope refer to condition where the slope is already failed due to landslide activity. The outcome highlights the advantages of considering the geophysical parameters and deriving elastic moduli in defining the subsurface behaviours. The study provides insights into how spatial distributions of geophysical properties used to minimise the uncertainty in the ground models. Besides that, cross-plot analysis with the development of 2-D cross-plot model was introduced based on the integration of resistivity and velocity values in order to enhance the subsurface resolution besides providing comprehensive subsurface images.

## **1.2 Landslide overview**

There are numerous landslide tragedies in Malaysia recorded and involved a high number of fatalities and economic losses. Slope failure events occurred are mostly triggered by heavy rainfall due to the tropical rainforest climate with relatively high temperature and rainfall throughout the year. In a tropical region like Malaysia, rainfall-induced landslide becomes common geohazard phenomenon where the soil typically deposits by residual soils (Huat et al., 2005; Rahimi, 2010). The significant thickness of the unsaturated zone with deep groundwater table shows the features of

residual tropical soil (Rahardjo et al., 2009). Malaysia experiences hot and humid climate all year round with temperature 22-32 degree Celsius with annual rainfall from 200–250 cm and extremities during southwest (April-October) and northeast (October-February) monsoons (Yusoff et al., 2016). The formation of residual soil is caused by intense chemical weathering due to the combination of climatic parameters. Under certain geological and topography effect, the rainfall becomes a major factor that triggered the occurrence of landslides involving both natural and cut slopes. The intense precipitation in highland area causes the situation to become more hazardous. Although the hilly area is stable of a certain range of water saturation, under critical limit, the shear resistance is enhanced due to effect of suction which creates an apparent cohesion between particles (Springman et al., 2003). Major landslides at local slope failure occur due to water saturation exceeds a critical limit in certain parts of the slope (Friedel et al., 2006). Based on a study conducted by Chigira et al. (2011), granitic rock is known to be very sensitive to weathering and vulnerable for mass sliding.

In a tropical region like Malaysia, deep weathering profile undergo a thickness up to 100 m. The nature of weathered material and mass structure highly control the failure mechanism. The extensive weathering effect causes the soil at the top layer to form loose layer and resulting it to slide. The high erodibility with the existence of relict discontinuities, sharp soil-rock boundary, dynamic weathered material under the saturated condition and the inhomogeneity of weathering structures will lead to frequent slope failure events. The presence of a fracture and structural discontinuity causes the cohesion and internal friction decreases or reduced by severing bonds between particles and created the discrete failure surfaces (Terzaghi, 1962; Carson & Kirkby, 1972). The understanding of the unsaturated soil mechanics is important in

investigation of rainfall-induced landslide mechanism, as shown in Figure 1.1. The phenomena occur mainly initiated by loss of matric suction in the unsaturated zone during rainfall infiltration as resulting in reducing in shear strength (Lu & Godt, 2008; Travis et al., 2010). Therefore, evolving scientific comprehension of the geological and physical process of earth's rheology is vital to assess and develop a predictive model for hazard problems.

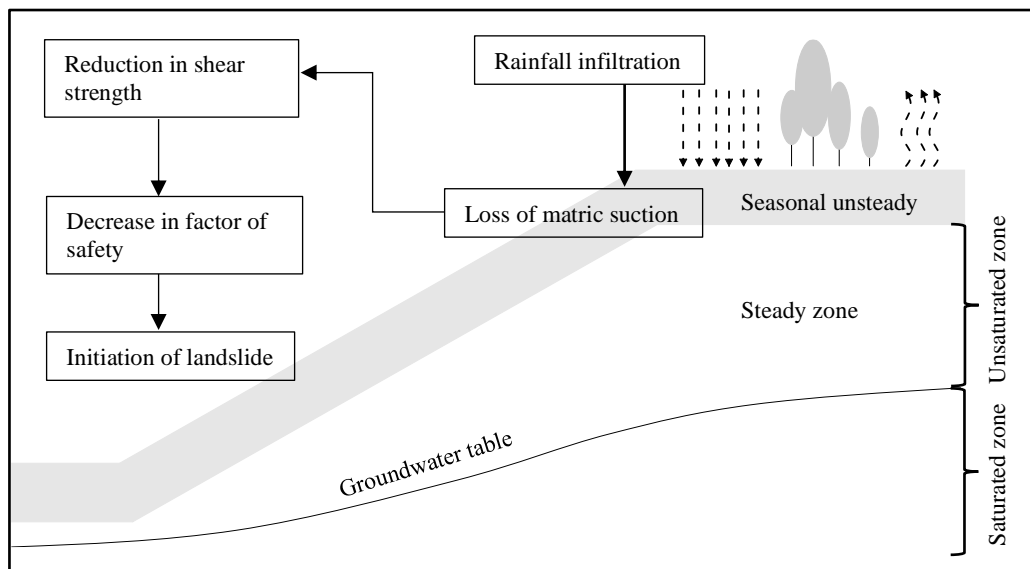


Figure 1.1 An overview of rainfall-landslide mechanism (Yeong, 2012)

### 1.3 Problem statement

Slope failure or landslides has been studied for several decades using multidisciplinary approaches (Ventura et al., 2011; Guzzetti et al., 2012; Travelletii et al., 2013; Pazzi et al., 2017). The methods provide comprehensive knowledge of the slope behaviour including characterisation of failure area, affected volume and factor of controlling mechanism. Conventional assessment like geotechnical investigations and remote sensing provide particular characteristic of the subsurface based on the parameters and the limitations of the methods. Geotechnical investigations give verifiable information on the subsurface features but in a limited point-scale as it requires more boreholes for the wider area. Remote sensing has been proven to provide

large scale information regarding surface features of the slope but inadequate resolution in characterising the subsurface geometries, which plays a vital role in landslide mechanism. Therefore, geophysical approaches were implemented to provide comprehensive data resolution in characterising the subsurface properties of the geomaterials with high level of accuracy. Due to the ability of the methods which provide a significant depth of investigation with promising data resolution such as defining plane weakness of the geomaterial, it shows high efficiency for methods to be considered. The justification of the geophysical parameters with geotechnical and hydrological properties is needed to provide comprehensive interpretations where those properties play an important role in landslide mechanism. However, without any correlation and validation with supported data, the results are vulnerable to misinterpretation. Hence, a cross-plot analysis was introduced as an alternative method to integrate two or more different parameters as to reduce the ambiguity of the data. The analysis provides direct visual interpretations based on the integrated parameters which enhance the subsurface images. The 2-D cross-plot model provides insights into how the spatial distribution of landslide mechanism was identified with the volume of mass sliding successfully determined. The accurate identification of a sliding plane reduces the error during the volumetric estimation.

#### **1.4 Objective of the research**

The research involves several geophysical methods with validation of several supported data from geotechnical and hydrological parameters in order to study the subsurface of the landslides area based on the following objectives:

- i. To characterise the slope/landslide body using 2-D resistivity, seismic refraction and MASW methods based on different types of slope condition;



- ii. To validate the results from geophysical methods with supported data from geotechnical and hydrological parameters; and
- iii. To integrate different geophysical parameters using cross-plot analysis with the development of 2-D cross-plot models for enhancing subsurface images and volume evaluations of mass sliding.

### **1.5 Scope of the research**

This research involves geophysical approaches in characterisation of the subsurface features of the body of the landslide based on different slope conditions which are stable, critical, and failure slope. The USM-Archaeology and Lojing-Cameron Highland study areas represent the stable and critical slope condition, respectively. Meanwhile, the failure slope was represented by study area of Hulu Yam and Bkt Antarabangsa. The geophysical methods, which are 2-D resistivity, seismic refraction, and MASW were applied in the study area. The research aims to provide insight into the landslides/slope mechanism based on the geophysical parameters and validate the data using geotechnical and hydrological parameters. The laboratory analysis and elastic modulus derivation were involved in providing exhaustive and realistic interpretations. Furthermore, this research frameworks also introduced a comprehensive and integrated method between different geophysical parameters using 2-D cross-plot models. A test model was analysed to obtain initial interpretation and validation from borehole information. The cross-plot analysis was applied at the selected study areas, and the results obtained were used to analyse the properties of the subsurface with the estimation of the landslide volume.

## **1.6 Novelty of the research**

Geophysical approaches were applied to study the soil characteristics of failure zones in order to create an image of the soil properties by providing realistic data interpretation. The outcome of the works highlights the advantages of considering geophysical parameters in defining the subsurface behaviours to be cost-effective and provided a high spatial resolution of the sliding mass geometry with validation from geotechnical and hydrological data. This research also introduces an alternative integrated method with development of 2-D cross-plot model using different geophysical parameters. The models successfully mapped the subsurface properties as the vulnerable layers were identified. The study provides insights into how spatial distributions of elastic properties can be used to minimise the uncertainty in the ground models. Besides that, the cross-plot models between the integration of resistivity and seismic results show an informative technique in enhancing subsurface resolution with the volume of mass sliding were successfully calculated.

## **1.7 Thesis outline**

In this thesis the research framework, data analysis, interpretation and the outcome of this research were presented with the following chapter as described below.

Chapter 1 briefly describes the background of the study, the problem statement, the research scope, and the objectives of the research with the significance of the research outcome. It also describes the general overview of the landslides in Malaysia region with previous research findings. Chapter 2 discusses the general theory of geophysical and geotechnical method with the background of the methods and previous research related to the landslides study cases. Furthermore, Chapter 3 defined the methodology and typology of the research framework, including the study area,

data acquisition and processing stages with a general overview of fundamental background. This chapter also discusses the required information and data needed for cross-plot analysis as well as to develop the 2-D cross-plot model. Next, chapter 4 discusses and explains all the collected information and results for each case study. The subsurface of landslide characteristic with the correlation of geotechnical and hydrological parameters were briefly explained. The integrated geophysical parameters using cross-plot analysis were presented with the volumetric of mass sliding were well defined. Lastly, the conclusion and recommendation are presented in Chapter 5.

## **CHAPTER 2**

### **LITERATURE REVIEW**

#### **2.1 Introduction**

The destabilisation and mass movement of soil and rock on slopes occurs as a common phenomenon across the globe and causes loss of life and severe damage to the property and infrastructure in the affected areas (Petley, 2012; Froude & Petley, 2018; Whiteley et al., 2019). A detailed investigation on the landslides provides essential information including soil and rock characteristics, landslide geomorphology and other parameters. The investigations of subsurface landslide features are indispensable for performing a forward modelling and subsequently predicting the potential slope failures including the run-out distance of the mass movement and the mobilised volume (Malet et al., 2005; Rosso et al., 2006). The geophysical approaches were capable of identifying the spatial variations of physical parameters of the landslide subsurface by physical property contrasts, including the physical extent of the landslide, slip surface, lithological contact and distribution of the movement of moisture throughout landslide body (Everett, 2013; Parsekian et al., 2015; Whitley et al., 2019). The features of a typical landslide mechanism which can be identified and assessed using geophysical method are shown in Figure 2.1. Nowadays, the application of geophysical approaches in landslides characterisation has become increasingly common. The multi-approach method for landslide investigation allows an even better evaluation of the internal structure by overcoming the limitations of single-method approaches (Schrott & Sass, 2008).

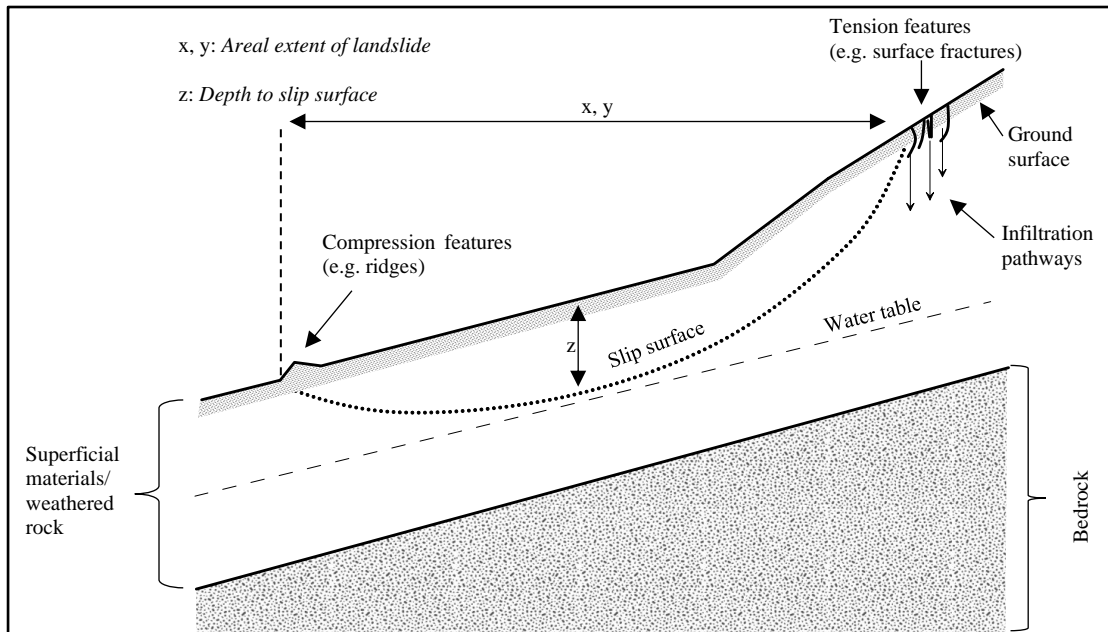


Figure 2.1 Schematic diagram of a landslide system, showing the major landslide setting features that can be investigated and assessed using geophysical methods (Whitley et al., 2019)

## 2.2 Basic theory of resistivity

The resistivity of the material is defined as resistance of a cylinder with a cross-section of unit area per unit length. Figure 2.2 shows the resistance,  $R$  of conducting cylinder with length,  $L$  and cross-sectional area,  $A$ . The resistivity,  $\rho$  of the conductor and its relationship with the geometric parameters are expressed using Equation 2.1. Resistivity survey is generally used to characterise the subsurface resistivity distribution based on the measurements on the ground surface. The resistivity value is related to some of the geological parameters, including porosity, fluid content and degree of water saturation in rock. In the resistivity method, electric currents are passed through the surface of the electrodes that are inserted into the ground, thereby resulting in a potential difference. The differences in the patterns of potential difference in the homogenous ground provides information and electrical properties of the subsurface inhomogeneities (Kearey et al., 2013).

$$R = \rho L/A \quad (2.1)$$

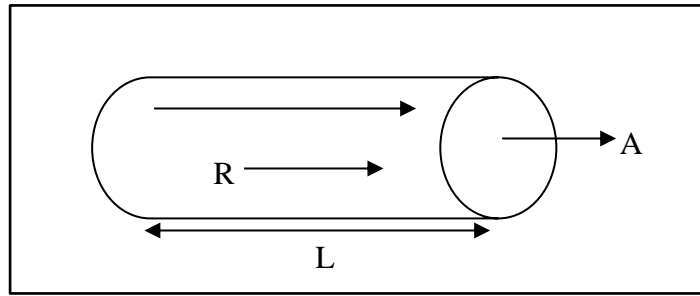


Figure 2.2 Electrical resistivity with the relation of resistance (R), area (A), and length (L)

The Equation 2.1 shows that the resistance, R is proportional to the length, L, and inversely proportional to the cross-sectional area, A, of the conductor. The SI unit of resistivity is ohm.meter ( $\Omega\text{m}$ ). According to Loke (2015), in the resistivity method, the current is injected into the ground through two current flowing electrodes: C1 and C2. The potential difference is measured using two potential measurement electrodes, namely P1 and P2. Figure 2.3 shows the configuration of a four-electrode array.

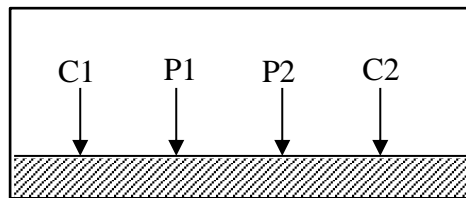


Figure 2.3 A conventional four-electrode array (Loke, 2015)

The apparent resistivity,  $\rho_a$  is calculated based on Equation 2.2.

$$\rho_a = kV_g/I \quad (2.2)$$

where k is a geometric factor that depends on the arrangement of the four electrodes. In resistivity survey, the value of 'k' plays an important role, wherein the depth of penetration of resistivity sounding depends on the spacing of electrode, which is referred to as 'k' value. Figure 2.4 shows the common electrode array used in the 2-D resistivity survey for different electrode spacing.

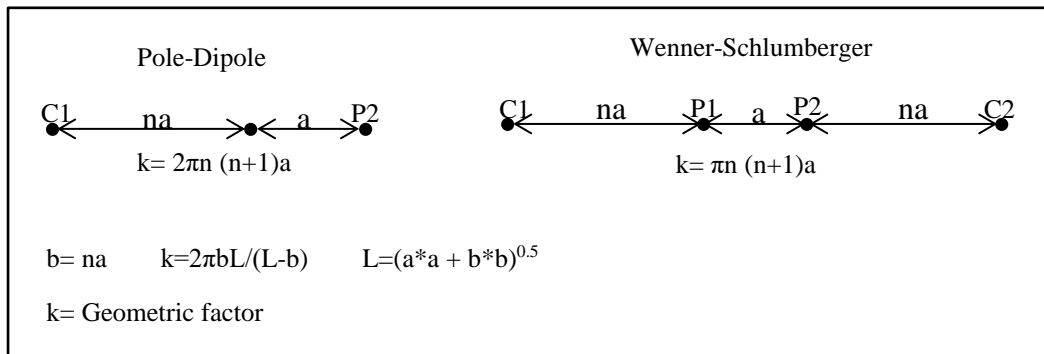


Figure 2.4 Common array used in an electrical survey with different geometric factor (Loke, 2015)

According to Loke (2015), the calculated value is not the true resistivity but refers to an apparent value. In order to obtain a true subsurface resistivity, an inversion process must be carried out using computer software. In the homogenous ground, the current is allowed to flow uniformly across a hemispherical shell centered on the source, as shown in Figure 2.5. The depth of penetration is proportional to the electrode spacing. The resistivity value of the homogenous ground should be constant and independent of electrode spacing and surface location. When non-homogenous subsurface exists, the resistivity will differ relative to the electrode position. The value of calculated resistivity is known as apparent resistivity (Kearey et al., 2013).

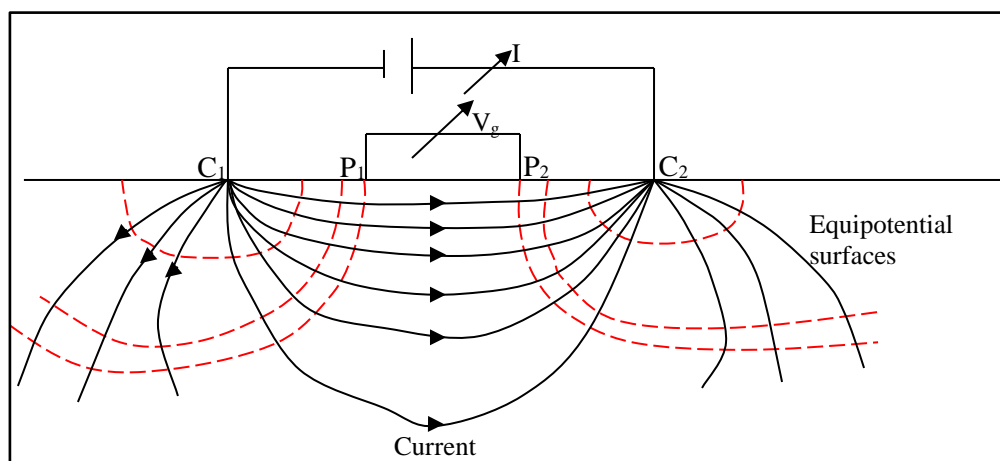


Figure 2.5 Illustration of current flow in the homogeneous subsurface (modified from Loke, 2015)

### **2.3 Basic theory of seismic refraction**

The seismic refraction method is one of the geophysical methods applied to study the earth's behaviour in identifying the characteristics, lithology, and other properties. This method involves the estimation of P-wave velocity ( $V_p$ ) of the earth near-surface material and has also been used to investigate landslides since the early 1960s (Narwold & Owen, 2002). Refraction survey has been used to estimate the depths to the failure and lateral extent of the landslide (Al-Saigh & Al-Dabbagh, 2010; Abidin et al., 2012a; Yilmaz & Kamachi, 2018) based on the differences in the physical properties of the sliding materials and the underlying undisturbed sediments or bedrock that result in different seismic velocities (Abramson et al., 2002). The underlying principle behind the seismic refraction method is the measurement of travel times of the seismic waves refracted at the interfaces between the subsurface layers of different velocities. The seismic energy generated by a seismic source ('shot') located on the surface radiates outward from the shot point spreading in all directions. The wave travels directly through the upper layer (direct arrivals), or it may travel down to and then laterally along with the high-velocity layers (refracted arrivals) before bouncing up and coming back to the surface (Figure 2.6). A critical refracted wave travels along the interface between layers and is refracted back into the upper layer at the critical angle. The waves refracted back into the upper layer are called head waves. The thickness and velocity of the material above and below an interface can be calculated by determining the arrival times of the direct and refracted waves from the seismic section (Saad et al., 2017). Hence, the final output comprises a depth profile of the refractor layers and a velocity model of the subsurface.



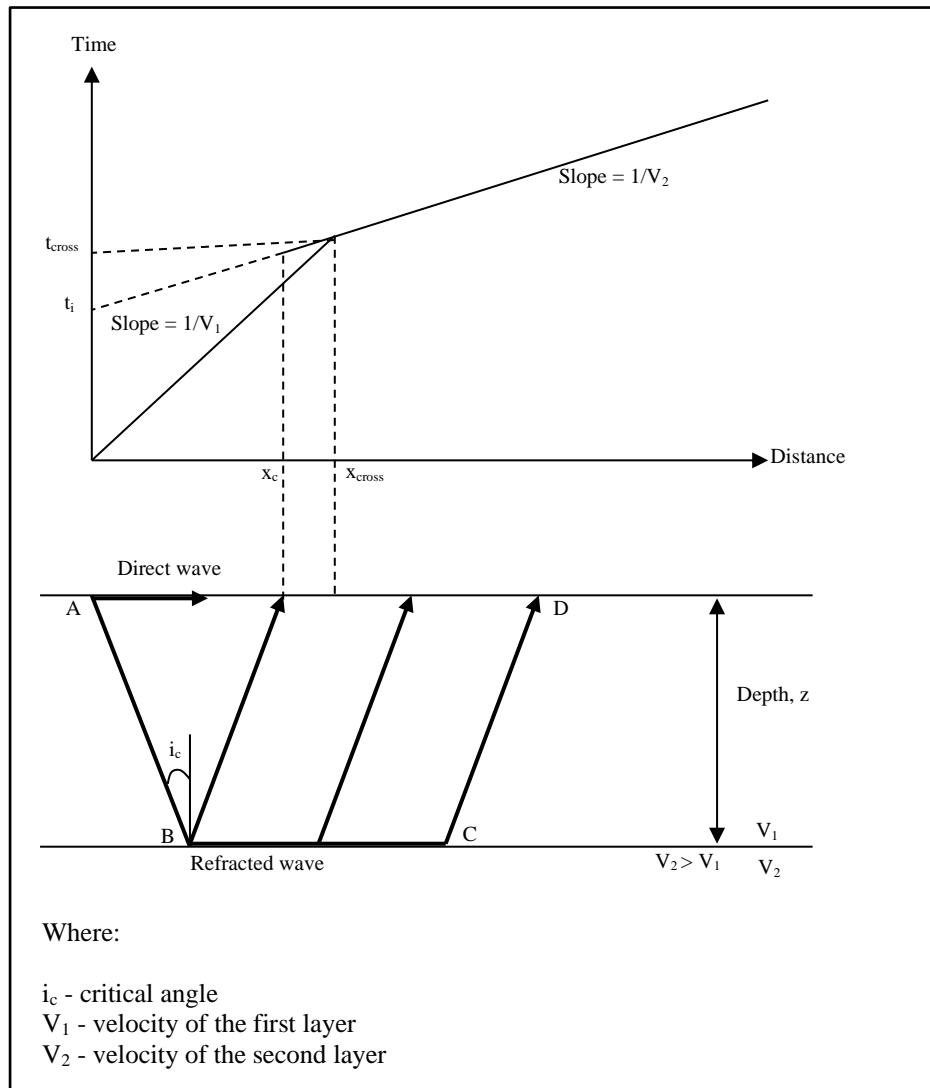


Figure 2.6 Travel time of seismic waves

## 2.4 Basic theory of multi-channel analysis of surface wave (MASW)

Surface wave analysis methods are based on the dispersive properties of surface waves in a vertically heterogeneous medium. Generally, the analysis is carried out utilizing Rayleigh waves as they were easy to be generated and be detected on the ground surface by low-frequency geophones (Socco et al., 2010) as a result of the interaction of P-waves ( $V_p$ ) and  $S_v$ -waves ( $V_{s-v}$ ) with the surface of the earth (Aki & Richards, 1980). Rayleigh waves velocity is generally observed to increase with depth (i.e., waves with longer wavelength (lower frequency) propagate faster than the shorter

wavelength (high frequency). The relationship between frequency ( $f$ ), Rayleigh wave phase velocity ( $V_r$ ), and wavelength ( $\lambda$ ) is given in Equation 2.3 (Kramer, 1996).

$$f = \frac{V_r}{\lambda} \quad (2.3)$$

The phase velocity of a Rayleigh wave component propagating through a layered medium is determined by the average stiffness and the average density of the soil layers that it travels (Everett, 2013). Figure 2.7 shows a schematic diagram of wave propagation.

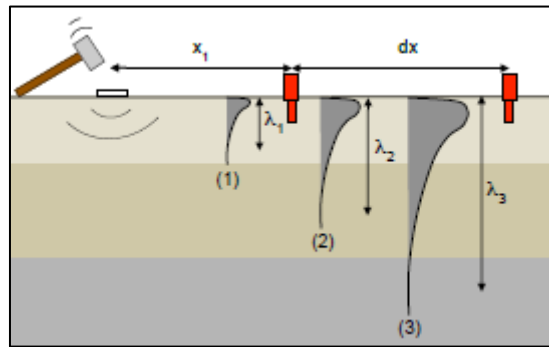


Figure 2.7 Rayleigh wave component with different wavelength propagating through a layered medium. Wave components with different frequency reflect soil properties at diverse depth

Multi-channel analysis of surface waves (MASW) is a non-invasive method of estimating the shear-wave velocity profile from surface wave energy. The method has been increasingly applied to geotechnical and engineering geology (Rehman et al., 2016; Arisona et al., 2017; Anukwu et al., 2018a, Anukwu et al., 2018b) and various shallow geophysical sounding (Bajaj & Anbazhagan, 2017; Pamuk et al., 2016; Mi et al., 2017). The most common uses of the surface wave's dispersive properties are to obtain  $V_s$  profiles by analysing plane waves, while fundamental Rayleigh waves carry more than 2/3 of total seismic energy generated. In a layered media, the frequency of a surface wave is related to the elastic and physical properties of the material (Lee et al., 2002). In such a context, the inversion technique was developed to retrieve information

measured from surface wave dispersion. Dispersion is a term that describes the change of phase velocity with frequency. In the case of elastic half-space (i.e., no velocity changes with depths), no surface wave dispersion will occur. Dispersion will occur only when velocity changes vertically. At high frequencies, the wavelengths are short, and the propagation velocity is controlled by the wave-speed of the shallow soil layers (which are usually of low speed). As the frequencies decrease, the wavelengths increase, causing the wave to penetrate to deeper layers with higher velocities (Khalil et al., 2017).

## **2.5 Elastic moduli for subsurface characterisation**

The body wave velocities of soil, which are the compressional wave ( $V_p$ ) and shear wave ( $V_s$ ), can be directly related to the medium of wave propagation's elastic moduli. The relationship between the elastic moduli and body wave velocities is widely utilized in the geophysical survey to obtain information on the spatial distribution of mechanical properties of the subsurface (Everett, 2013). The most commonly used moduli to characterize soil are the small strain shear modulus,  $G_0$ , and Young's modulus,  $E$  (either express in terms of undrained/total stress or drained/effective stress). Both of these moduli provide the measurement of material's stiffness and are defined as the ratio of stress to resulting strain along an axis resulting from shear ( $G_0$ ) or loading ( $E$ ) (Clayton, 2011; Mavko et al., 2020). Shear modulus also reflects the rigidity of the material that describes the ability of the material to resist shearing (i.e., change of the shape without change the volume). Thus, the shear modulus is equal to the ratio of shear stress to shear strain, while Young's modulus,  $E$ , is referred to as the compressibility behaviour. Both  $G_0$  and  $E$  are frequently used in the estimation of soil consolidation (Braja, 2008), deformation analysis (Clayton, 2011) as well as physical landslide modelling (Lacroix & Amitrano, 2013). Equations 2.4 and 2.5 show the relationship of

shear modulus and Young's modulus with the density,  $\rho$  of the material. Table 2.1 lists the general values of shear modulus for several types of soil.

$$G_0 = \rho v_s^2 \quad (2.4)$$

$$E = \frac{\rho v_s^2 (3v_p^2 - 4v_s^2)}{(v_p^2 - v_s^2)} \quad (2.5)$$

where;

$v_s$ = S-wave velocity  
 $v_p$ = P-wave velocity  
 $\rho$ = density

Table 2.1 General values of shear modulus for several soil types (Sabatini et al., 2002)

Soil Type	Shear modulus, $G_0$ (GPa)
Soft clays	0.00275-0.01375
Firm clays	0.0069-0.0345
Silty sands	0.0276-0.138
Dense sands and gravels	0.069-0.345

Another commonly used parameter in slope stability analysis is the Poisson's ratio,  $\nu$  (Martel & Muller, 2000; Ulehman et al., 2016a), which is linked to the stress field in the slope and degree of saturation of the soil material (Huang et al., 2012). In contrast to the shear and Young's moduli, no density estimation was required for the calculation of  $\nu$ , which highlights the benefit of considering Poisson's ratio (Equation 2.6) by eliminating the potential uncertainties rising from an assumed density. Table 2.2 lists the general values of Poisson's ratio for several types of soil.

$$\nu = \frac{v_p^2 - 2v_s^2}{2(v_p^2 - v_s^2)} \quad (2.6)$$

where;

$v_s$ = S-wave velocity  
 $v_p$ = P-wave velocity

Table 2.2 General values of the Poisson's Ratio for several soil types (Braja, 2008)

Soil type	Poisson's Ratio
Loose sand	0.2-0.4
Medium sand	0.25-0.4
Dense sand	0.3-0.45
Silty sand	0.2-0.4
Soft clay	0.15-0.25
Medium clay	0.2-0.5

## 2.6 Shear strength of the soil

Shear strength of the soil mass refers to the internal resistance per unit area that the soil mass can offer to resist failure and to slide along any plane inside it (Braja & Sivakugan, 2015). It measures the soil resistance to deformation by continuous displacement of its soil particles. In 1900, Mohr presented a theory for rupture of a material relating the normal stress and shear stress on a failure plane as a linear function (Equation 2.7 and Figure 2.8). Saturation of soil slope will reduce the soil strength, which will lead to numerous collapses and failures of the slopes. Strength is the measure of the maximum stress state that can be induced in a material without it failing; fundamentally, it is the ability to sustain shear stress that provides the strength (Whitlow, 2004). The shear strength within a soil mass is essentially due to the development of frictional resistance between the adjacent particles. Shear strength in soils depends primarily on the interactions between the particles, and a failure occurs when the stresses between the particles are high as they slide or roll past each other. Soil derives its shear strength as cohesion and frictional component. Table 2.3 shows typical drained shearing angles of friction for different soil types (Whitlow, 2004).

$$\tau_f = c + \sigma \tan \phi \quad (2.7)$$

where;

$c$  = cohesion

$\phi$  = angle of internal friction

$\sigma$  = normal stress on the failure plane

$\tau_f$  = shear stress at failure

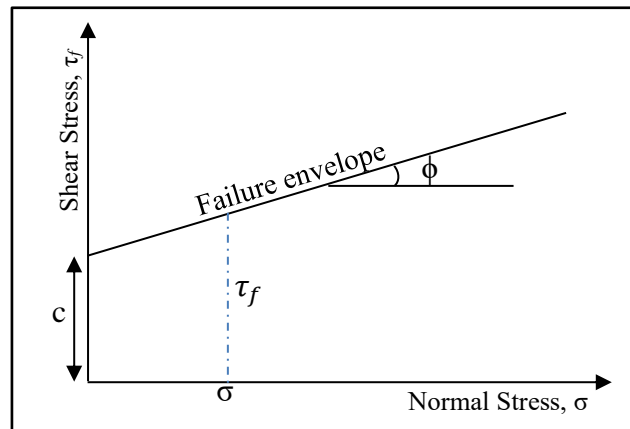


Figure 2.8 Mohr-Coulomb failure criterion

Table 2.3 Shearing angle of friction for soil types (Whitlow, 2004)

Soil types	$\phi$ (deg)
Sand: Rounded grains	
Loose	23-30
Medium	30-35
Dense	35-38
Sand: Angular grains	
Loose	30-35
Medium	35-40
Dense	40-45
Gravel with some sand	34-48
Silts	26-35

## 2.7 Overview of landslide in Malaysia

Malaysia is located in the Southeast of Asia, occupying about 330200 km<sup>2</sup>. The entire country is divided into two main regions, Peninsular Malaysia and East Malaysia. The geographic position subjects the country to a steamy, hot, and humid climate throughout the year with yearly monsoons from the southwest from April to October and from the northeast from October to February. Also, Malaysia has not experienced

strong/major earthquakes, but large-scale landslides still occur due to mainly gravity-induced events at times of heavy and prolonged rainfall. Due to rapid development since the 1980s, strategic and suitable low-lying areas have become increasingly unavailable for development. The development of highland or hilly terrain has increased, particularly in areas adjacent to densely populated cities, thereby exposing urban communities to increased landslide occurrences. The development of hill land leads to severe irreversible effects on its immediate environment and the surrounding environment downstream (Rahman & Mapjil, 2017).

In the report titled 'National Slope Master Plan (2009-2023)', a total of 49 cases of massive landslides have been reported, out of which is 88% were attributed to the manmade slope (JKR, 2009a,2009b). The hills, which are usually categorized into dangerous slopes (20-30 degrees) and critical slopes (>30 degrees), should be avoided from development. Mohktar (2006) highlighted that the main factors contributing to slope failure/landslide at several sites in the hillside are rainfall and stormwater activities. The most common type of landslide in Malaysia is a shallow landslide where the slide surface is usually less than 4 m deep and occurs during or immediately after intense rainfall (Rahman & Mapjil, 2017). The high temperatures throughout the year with prolonged rainfall cause intense chemical weathering and favours the formation of thick residual soil profiles. With this set of climate and geological conditions, combined with other causative factors, landslides are thus one of the most destructive natural disasters in Malaysia (Bujang et al., 2008). The statistics of the cases reported by Gue and Tan (2007) mentioned that incompetency would lead to landslide events in addition to the poor design of the slope structures (Table 2.4). The underestimation of the existing groundwater tables and inadequate surface drainage capacity also weighed in among the factors causing landslides.

Table 2.4 Reported cases of landslide in Malaysia in year of 2000-2006 (Gue & Tan, 2007)

Causes of Landslides	Number of Cases	Percentage (%)
Design error	29	60
Construction errors	4	8
Design and constructions errors	10	20
Geological features	3	6
Maintenance	3	6

## 2.8 Previous study

The previous study was discussed based on the assessment of landslide from multi-disciplinary approach with the implementation of cross-plot analysis for subsurface characterization based on the following subsection.

### 2.8.1 Overview of landslide assessment

Slope failure is a complex phenomenon that may trigger the occurrence of landslides due to several factors and become one of the major geomorphic processes that affect the evolving landscape of the mountainous region, favouring disastrous phenomena. The broad or small scale of landslide refers to a widespread natural process resulting from the downward and outward movement of slope-forming materials, including sculpting the landscape. The characterization of landslides in heterogeneous conditions becomes one of the biggest challenges as the assessment requires extensive data ranging from multidisciplinary approaches as the measurement of geological and hydrological parameters (Pazzi et al., 2019). Conventional methods of geomorphology survey, geotechnical investigation, and more recent methods of remote sensing, aerial photography, and synthetic aperture radar interferometry, can be employed to obtain and analyse the information required regarding the landslides properties (Travelletii et al., 2013; Pazzi et al., 2017). Each method allows the study of specific triggering factors



or particular physical features based on the parameter and the method's ability. Satellite and airborne methods (i.e., GPS and digital aero photogrammetry) are also helpful in providing useful information regarding the surface characteristics of the slope including the geomorphological features, areas of extension of the landslide body, superficial displacement, and velocity (Ventura et al., 2011; Guzzetti et al., 2012). However, in most cases, all of this information does not include the subsurface features, which play a vital role in landslide characteristics. Direct ground-based techniques (i.e., piezometer and inclinometer) give verifiable and reliable information on the mechanical and hydraulic characteristics of the terrains affected by the landslides but at discrete points of the subsurface (Marcato et al., 2012). The application of geophysical approaches has witnessed an exponential increase for detailed subsurface characterization, localization of sliding surface, evaluation of the emergence and growths of fractures, and the understanding of water dynamics and possible reactivation by rainfall (Pazzi et al., 2019). The information obtained from geophysical surveys is used as an input for defining ground models of landslides and, consequently, to perform slope stability assessment (Whiteley et al., 2019).

Landslides activities in weathered granitic rocks are strongly affected by weathering types and have been documented for tropical and humid regions. Based on a study conducted by Chigira et al. (2011), granitic rock is known to be very sensitive to weathering and vulnerable to mass sliding. In a wet tropical region in Malaysia, a deep weathering profile will exhibit a thickness of up to 100 m. The mechanism of failure is highly controlled by the nature of weathered material and its mass structure. In 1993, Malaysia witnessed major slope failure disasters of Bkt Antarabangsa involving loss of lives and property damages. Komoo (1997) shows that weathered granitic materials may contribute as a major factor for a landslide to occur. The material

was classified as porous, easy to crumble, and inherited the plane of the parent rock's weakness. An extensive weathering profile of soil changed the condition, transformed the granite into residual soil, and weathered granite materials. The unstable condition with loose materials and increased accumulation of water triggered the occurrence of a landslide. In a revisit study at Bkt Antarabangsa by Lim et al. (2019), there were numerous evidence showing that the lands had significantly been battered and modified since the last 50 years before the landslides occurred. Extensive land exploitation, construction practices, construction on landslide affected terrains, or previously modified land slope had significantly contributed to recurring instances of landslide occurrence. The study shows that climate-induced geological factors (weathered granitic terrain) and lithological relics contributed to the predisposing factor, and the changes in land-use ascribed to disturbances in the terrain due to human habitation may also affect the occurrence of landslides. The site is an example of human-induced landslide disasters, which is a consequence of improper land use management and construction practices.

The infiltration of rainfall into the soil and its effect on slope failure has been of particular interest for the past few years (Irfan et al., 2017; Chen et al., 2018,2019; Jing et al., 2019). Rahardjo et al. (2007) conducted a series of parametric studies to understand the hydrological and geotechnical parameters on rainfall-induced instability. The study inferred that rainfall intensity, soil properties, groundwater table, and slope geometry played an important role in the rain-induced instability of the slope. The continuous infiltration of rainwater will increase the pore-air pressure and decrease the matric suction, compromising slope stability (Sun et al., 2015, 2016). The process causes a change in effective stress, which produced variations in the porosity of the soil (Sun et al., 2016).

According to Collins and Znidarcic (2004), two distinct failure mechanisms have been observed in the event of rainfall-induced landslides. For the first mechanism, a significant build-up of positive pressures was observed in a low area on the slope or along with the soil/bedrock interface. Movements along the sliding surface lead to liquefaction along with it, resulting in rapid movements, long run-out distances, and finally, complete liquefaction of the failed mass occurred (Wang & Sassa, 2001). In the second mechanism, the soil was in an unsaturated state, and slope failure was mainly due to rainfall infiltration and a loss in shear strength when soil suctions are decreased or dissipated (Fourie et al., 1999). Infiltration and near-surface flow increased pore water pressure, causing the stress path to move nearly horizontally to intersect a failure envelope, initiating a slope failure. In unsaturated loose soils, suction decreases, and coupled volumetric collapse may involve the failure process (Olivares & Picarelli, 2003). Landslides in weathered granitic rocks for tropical and humid regions have been well understood as the phenomenon is strongly affected by the type of weathering.

Furthermore, the geophysical methods were included in landslide evaluations since this method was beneficial in identifying the petrophysical properties of subsoil, such as seismic wave, electrical resistivity, and dielectric permittivity (Travelletti & Malet, 2012). In-situ geophysical methods, of resistivity and seismic refraction measurements, are capable of evaluating the physical parameters directly or indirectly, including the lithology of the subsurface, hydrology, and geotechnical characteristics (Perrone et al., 2014). These methods are less invasive and provide comprehensive information on a large soil volume, thus overcoming the point-scale features of geotechnical measurements. The successful geophysical methods were evident with significant contrast present among the physical properties of different lithological units (Pazzi et al., 2019).

Nowadays, the geophysical method has been extensively utilized in slope failure assessments. Dostal et al. (2014) and Ng et al. (2015) conducted 2-D resistivity measurement intending to characterize the subsurface layer of the slope for remedial works to identify the shear zone. The outcome shows that low resistivity zones face the risk of slope failure, which demand remedial measures. The prospection zone of loose soil with high resistance was clearly visible and indicated that the landslides in history consisted of cohesive deposit materials in relic landslide as conducted by Kaczmarek et al. (2014). The 2-D resistivity and geotechnical method was successfully applied to estimate the geometry, thickness, and depth of the landslide's failure zone (Maniruzzaman et al., 2017). The relationship between friction angles for various soil properties was established by simple regression analysis from apparent resistivity data. The results revealed that the increase in water content in the slide zone reduced the shearing resistance's effectiveness and increased the sliding movement. Abidin et al. (2017) and Muztaza et al. (2017) showed that the 2-D resistivity study could determine the subsurface geometry with the factors contributing to landslide events. The existence of weak zones represented low resistivity values due to high water content or highly conductive materials (Abidin et al., 2017). The study showed that heavy rainfall and existing geological structure (weakness zone) played a critical role in contributing to the landslide occurrence. This finding proved that this method could predict the landslide's features to assist the conventional borehole data. The presence of weathered granite, fracture, and boulders would be an indicative factor for landslide events (Muztaza et al., 2018).

In 2011, Clarke and Burbank conducted a seismic refraction study to calculate the depth, densities, and gradient of the bedrock fracture. It revealed two subsurface scenarios: the bedrock that uniformly fractured with depth and the bedrock fractured